



**HAL**  
open science

# A general pattern of non-spiking neuron dynamics under the effect of potassium and calcium channel modifications

Loïs Naudin, Laetitia Raison-Aubry, Laure Buhry

## ► To cite this version:

Loïs Naudin, Laetitia Raison-Aubry, Laure Buhry. A general pattern of non-spiking neuron dynamics under the effect of potassium and calcium channel modifications. 2022. hal-03751106

**HAL Id: hal-03751106**

**<https://hal.science/hal-03751106v1>**

Preprint submitted on 13 Aug 2022

**HAL** is a multi-disciplinary open access archive for the deposit and dissemination of scientific research documents, whether they are published or not. The documents may come from teaching and research institutions in France or abroad, or from public or private research centers.

L'archive ouverte pluridisciplinaire **HAL**, est destinée au dépôt et à la diffusion de documents scientifiques de niveau recherche, publiés ou non, émanant des établissements d'enseignement et de recherche français ou étrangers, des laboratoires publics ou privés.

1 A general pattern of non-spiking neuron dynamics  
2 under the effect of potassium and calcium channel  
3 modifications

4 Loïs Naudin<sup>1\*</sup>, Laetitia Raison-Aubry<sup>1</sup>, and Laure Buhry<sup>1\*</sup>

5 <sup>1</sup>Laboratoire Lorrain de Recherche en Informatique et ses Applications,  
6 CNRS, Université de Lorraine, Nancy, France

7 \*Corresponding author: lois.naudin@gmail.com, laure.buhry@loria.fr

8 August 13, 2022

9 **Abstract**

10 Electrical activity of excitable cells results from ion exchanges through cell mem-  
11 branes, so that genetic or epigenetic changes in genes encoding ion channels are likely  
12 to affect neuronal electrical signaling throughout the brain. There is a large litera-  
13 ture on the effect of variations in ion channels on the dynamics of spiking neurons  
14 that represent the main type of neurons found in the vertebrate nervous systems.  
15 Nevertheless, non-spiking neurons are also ubiquitous in many nervous tissues and  
16 play a critical role in the processing of some sensory systems. To our knowledge,  
17 however, how conductance variations affect the dynamics of non-spiking neurons has  
18 never been assessed. Based on experimental observations in the biological literature  
19 and on mathematical considerations, we first propose a phenotypic classification of  
20 non-spiking neurons. Then, we determine a general pattern of the phenotypic evo-  
21 lution of non-spiking neurons as a function of changes in calcium and potassium  
22 conductances. Furthermore, we study the homeostatic compensatory mechanisms of  
23 ion channels in a well-posed non-spiking retinal cone model. We show that there is  
24 a restricted range of ion conductance values for which the behavior and phenotype  
25 of the neuron are maintained.

26 **Keywords:** non-spiking neurons; conductance variations; bifurcation; retina; *Caenorhab-*  
27

## 29 1 Introduction

30 Electrical activity of excitable cells results from ion flows through the cell membrane, such  
31 that genetic or epigenetic modifications of ion channel proteins are likely to affect electri-  
32 cal signaling throughout the brain. In particular, dysregulations of calcium and potassium  
33 channel functioning, and their possible impact on ion homeostasis, are implicated in a wide  
34 range of neurological and psychiatric disorders. Among them, we find neurodegenerative  
35 disorders such as Parkinson (Zhang et al., 2020; Hurley and Dexter, 2012), Huntington  
36 (Czeredys, 2020; Tong et al., 2014), or Alzheimer (Supnet and Bezprozvanny, 2010; Stutz-  
37 mann, 2021; Villa et al., 2020) diseases, and various psychiatric diseases (Zhang et al.,  
38 2006; Heyes et al., 2015; Zamponi et al., 2015; Yanagi et al., 2014). Therefore, ion channel  
39 modifications are likely to affect sensory system processing as well, altering the electrical  
40 activity not only of spiking neurons, but also of non-spiking neurons as suggested by elec-  
41 trophysiological studies of retinal activity in patients suffering from Parkinson, Alzheimer,  
42 and Huntington diseases, epilepsy, depression, and schizophrenia (Silverstein et al., 2020).

43 While spiking neurons are thought to convey a large part of the neuronal information via  
44 action potential propagation along axons, non-spiking neurons, instead, modulate analog  
45 signals (*i.e.* graded potential responses). More specifically, the amplitude and waveform of  
46 the action potentials are essentially invariant with respect to the amplitude, duration, and  
47 waveform of the stimulus, unlike graded potentials whose waveform depends directly on  
48 the stimulus (Lockery et al., 2009) (Figure 1.A). This type of response has the advantage  
49 of preserving information content, but, as a consequence, makes non-spiking neurons more  
50 sensitive to noise than spiking ones (Sarpeshkar, 1998).

51 Spiking neurons are often perceived as the only information processing component of  
52 the nervous system. However, in a large diversity of nervous tissues in both vertebrate  
53 and invertebrate species, non-spiking neurons are prominent, such as most of the retina  
54 neurons (Field and Chichilnisky, 2007), a majority of *C. elegans* neurons (Goodman et al.,  
55 1998), the motoneurons of the *Ascaris* worm (Davis and Stretton, 1989b,a), or many  
56 interneurons in insects and crustaceans (Roberts and Bush, 1981). These neurons have  
57 been proven to play a paramount role in the functioning of these nervous systems. For  
58 instance, depolarizing currents received by non-spiking interneurons can reset biological  
59 central pattern generator rhythms in insects (Bidaye et al., 2018). Also, they can suppress  
60 the appearance of irregular variations of neural activity in small networks of spiking neurons

61 (Koch et al., 1989). Last, they are central in neuronal integration (Roberts and Bush, 1981)  
62 and provide a determining mechanism for the control of motor behaviors (Burrows et al.,  
63 1988; Laurent and Burrows, 1989a,b).

64 Despite their differences in the characteristics of their electrical signals, spiking and  
65 non-spiking neurons share similar mechanisms for transmitting them by active and passive  
66 propagation. Indeed, both types of neurons exhibit similar ion channels on their mem-  
67 branes, including a large diversity of classical voltage-dependent ion channels which have  
68 been experimentally and genetically identified in different non-spiking cell types (Roberts  
69 and Bush, 1981; Van Hook et al., 2019). Therefore, to characterize the non-spiking behav-  
70 ior, several works have built conductance-based models (CBMs) of retina neurons (Usui  
71 et al., 1996; Liu and Kourennyi, 2004; Publio et al., 2006; Kamiyama et al., 2009) or *C.*  
72 *elegans* neurons (Nicoletti et al., 2019; Naudin et al., 2020, 2022a; Jiménez Laredo et al.,  
73 2022) for instance.

74 CBM is an accurate biophysical representation of the neuron in which every individual  
75 parameter and state variable have an established electrophysiological meaning. Therefore,  
76 it is broadly used to understand ‘low-level’ functions of neural systems (Eliasmith and  
77 Trujillo, 2014; O’Leary et al., 2015). In particular, it is been extensively used to describe  
78 the effect of conductance variations on spiking neuronal dynamics, both at the single-cell  
79 (Drion et al., 2015; Berry and Genet, 2021) and at the network levels (Giovannini et al.,  
80 2017; Aussel et al., 2018). Such computational works have also been widely employed to  
81 study the homeostatic compensatory mechanisms of ion channels in a neuron (Achard and  
82 De Schutter, 2006; Soofi et al., 2012; Alonso and Marder, 2019; Onasch and Gjorgjieva,  
83 2020). Indeed, much experimental evidence suggests that a given neuron can maintain a  
84 specific electrophysiological signature from different combinations of its individual compo-  
85 nents, *e.g.* ion channels (Goillard and Marder, 2021; Kamaledin, 2021). For instance,  
86 experimental measurements have shown two- to six-fold variability in ion channels in the  
87 same identified neuron from different crabs (Schulz et al., 2006).

88 To our knowledge, there is no equivalent computational work that has systematically  
89 described the effect of conductance variations on the dynamics of non-spiking neurons,  
90 and the possible resulting compensatory effects. Therefore, the aim of this paper is to  
91 determine the effect of calcium and potassium conductance ( $g_{Ca}$  and  $g_K$ ) variations on  
92 the dynamics of non-spiking neurons, based on experimental observations in the biological  
93 literature, and illustrated with a mathematical analysis of a well-posed non-spiking retinal  
94 cone model (Kourennyi et al., 2004). Then, we discuss the computational implications on  
95 the neuron dynamics of these variations, and we propose a general pattern of the evolution

96 of non-spiking neuron dynamics (or “phenotypes”) as  $g_{Ca}$  and  $g_K$  evolve. Ion conductance  
 97 variations could represent possible gain- or loss-of-function mutations in the genes encoding  
 98  $Ca^{2+}$  and  $K^+$  channel sub-units. Then, we study the possible compensations between  $I_{Ca}$   
 99 and  $I_K$  for which the quantitative behavior and phenotype of the neuron are maintained.

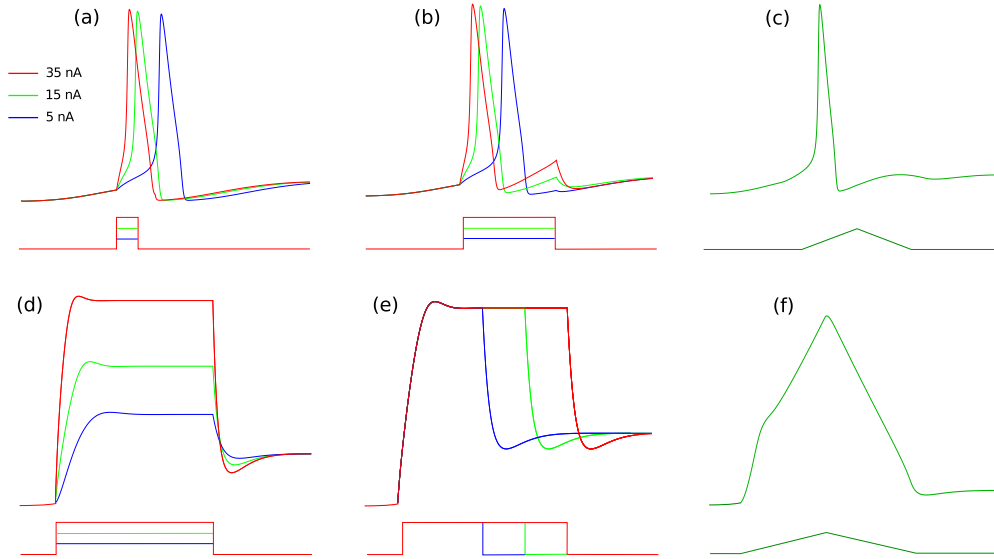


Figure 1: Difference of features between action potentials (a-c) and graded potentials (d-f). Action potentials have been simulated from the classical Hodgkin-Huxley model, while graded potentials have been obtained by reducing its maximal conductances  $g_{Na}$  and  $g_K$ . The amplitude and waveform of the action potentials are essentially invariant with respect to the (a) amplitude, (b) duration, and (c) waveform of the stimulus, while the amplitude and waveform of the graded potentials are dependent on the (d) amplitude, (e) duration, and (f) waveform of the stimulus. This figure has been reproduced from [Naudin et al. \(2022a\)](#) with the consent of the authors.

## 100 2 Results

101 **Phenotypic classification of non-spiking neurons based on the steady-state cur-**  
 102 **rent shape.** Two fundamental behaviors of non-spiking neurons exist: near-linear and  
 103 bistable. The near-linear behavior is defined by smooth depolarizations or hyperpolar-  
 104 izations from the resting potential, while the bistable one is characterized by nonlinear  
 105 transitions between the resting potential and a depolarized potential. Among the bistable  
 106 behaviors, we can distinguish two distinct phenotypes depending on whether the neuron has  
 107 one or two resting potentials. Therefore, we define three non-spiking neuron phenotypes:

108 near-linear (phenotype 1), bistable with one resting potential (phenotype 2), and bistable  
 109 with two resting potentials (phenotype 3). Figure 1. A shows experimental examples of  
 110 each phenotype.

111 What confers the neuro-computational characteristics to non-spiking neurons is the  
 112 steady-state current, noted  $I_\infty$  (see Naudin et al. (2022a) or Materials and Methods). As  
 113 a consequence, these three phenotypes can be distinguished on the basis of their steady-  
 114 state current shape (Figure 1.B). A monotonic steady-state current confers a phenotype  
 115 1 on the neuron. A N-shaped steady-state current with only one zero endows the neuron  
 116 with a phenotype 2. And a N-shaped steady-state current with two stable zeros gives  
 117 to the neuron a phenotype 3. In the following paragraphs, we investigate how variations  
 118 in calcium and potassium conductances are expected to affect the steady-state current,  
 119 and thus the phenotype, of non-spiking neurons based on experimental observations, and  
 120 illustrate this using a generic bistable non-spiking CBM.

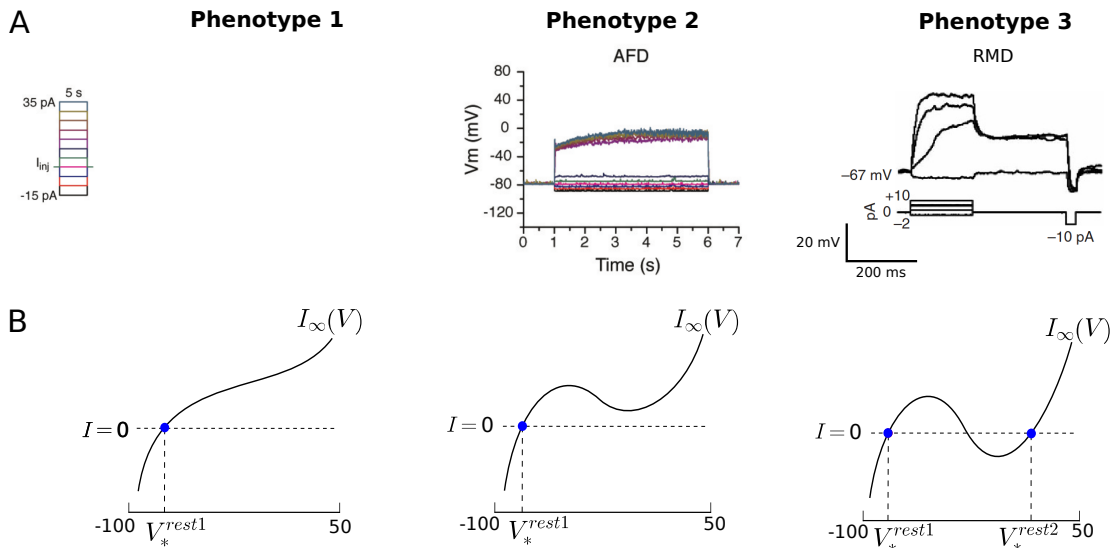


Figure 2: (A) Experimental voltage examples from *C. elegans* of each phenotype for a series of current injections starting from  $-15\text{pA}$  and increasing to  $35\text{pA}$  by  $5\text{pA}$  increments for the RIM and AFD neurons, and starting from  $-2\text{pA}$  and increasing to  $10\text{pA}$  by  $3\text{pA}$  increments for the RMD neuron. The experimental data of the RIM and AFD neurons have been reproduced from Liu et al. (2018), and from Mellem et al. (2008) for the RMD neuron with the consent of the authors. (B) Shape of the steady-state current curve associated with each phenotype.

121 **Changes in calcium and potassium conductances drive opposite transitions be-**  
 122 **tween neuron phenotypes.** In this paper, we use a well-posed retinal cone model (see

123 Materials and Methods) to illustrate and assess the effect of conductance variations on  
124 non-spiking neuronal dynamics. Since the steady-state current determines the qualitative  
125 characteristics and the phenotype of a non-spiking neuron, we observe its evolution as  $g_{Ca}$   
126 and  $g_K$  evolves. It can be seen in Figure 3 that the variations of  $g_{Ca}$  and  $g_K$  have opposite  
127 effects on the evolution of the steady-state current shape of the model. Indeed, the wild-  
128 type (WT) steady-state I–V relation ( $g_{Ca} = 4.92\text{nS}$  and  $g_K = 2\text{nS}$ ) exhibits a region with  
129 negative slope that becomes less and less steep and then disappears as  $g_{Ca}$  decreases or  
130  $g_K$  increases. In other words, the decrease of  $g_{Ca}$  leads to the transition from a phenotype  
131 3 to a phenotype 2 and then to a phenotype 1. The same phenotypic changes occur as  
132  $g_K$  increases, so that variations in  $g_{Ca}$  and  $g_K$  have opposite effects. This is consistent  
133 with experimental observations on the non-spiking bistable ASER neuron of *C. elegans*  
134 for which the negative slope region of its steady-state current is due to the opposition of  
135  $K^+$  and  $Ca^{2+}$  currents (Goodman et al., 1998). In addition, these authors show that the  
136 voltage-dependence of membrane current is similar in 42 unidentified neurons, suggesting  
137 that the ubiquitous flat region of the steady-state current in *C. elegans* neurons share the  
138 same common underlying mechanism (opposition of  $K^+$  and  $Ca^{2+}$  currents). A similar  
139 mechanism is described in vertebrate hair cells in which the flat region of their membrane  
140 current-voltage relationship results from a counterbalanced flow of  $I_K$  and  $I_{Ca}$  (Art and  
141 Goodman, 1996; Fettiplace, 1987). Furthermore, in a small group (15%) of thalamocorti-  
142 cal neurons, the low threshold T-type  $Ca^{2+}$ -current ( $I_T$ ) is also responsible for an intrinsic  
143 bistability (Hughes et al., 1999; Williams et al., 1997). Augmentation of endogenous  $I_T$   
144 by an artificial analog transforms all non-bistable thalamocortical neurons to bistable cells  
145 (Hughes et al., 1999), which is still consistent with results depicted in Figure 3 (left).

146 Last, it is worth noting that a new phenotype appears for very large values of  $g_{Ca}$  and  
147 very small values of  $g_K$ . Indeed, for these values, the steady-state current is N-shaped with  
148 a negative local maxima. This involves a hyperpolarizing voltage jump (Figure S1), in  
149 contrast to phenotype 2 which exhibits a depolarizing jump of the voltage. The shape of  
150 the steady-state current is similar to the phenotype 2 (N-shaped with only one zero) so we  
151 can name this one the phenotype 2\*. However, to our knowledge, this type of non-spiking  
152 behavior has never been observed experimentally.

153 In the following, we describe the computational implications of phenotypic transitions  
154 on the neuronal dynamics. As an illustration, we consider the decreasing variations of the  
155 calcium conductance  $g_{Ca}$ . Therefore, we first describe the computational characteristics  
156 of the wild-type neuron phenotype which is phenotype 3, and its phenotype 2 and then 1  
157 resulting from the decrease in  $g_{Ca}$  that would reflect calcium channel dysfunctions.

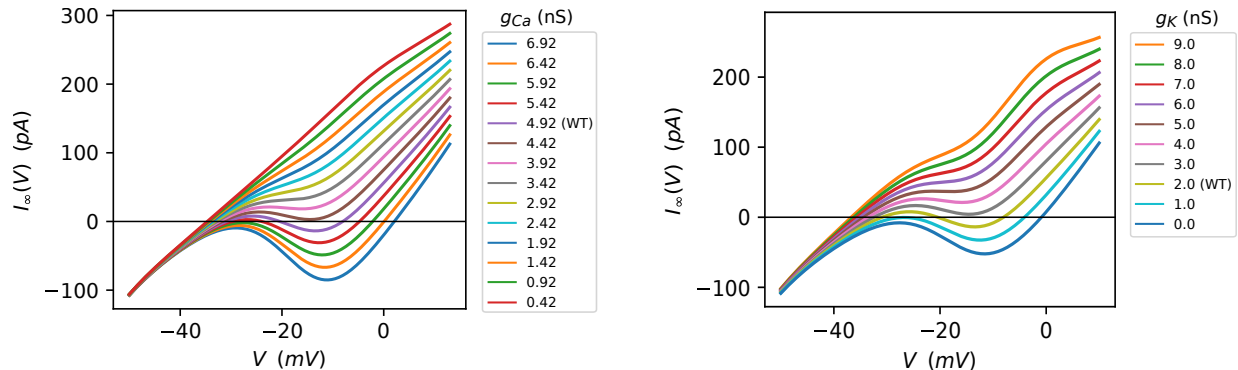


Figure 3: **Evolution of the steady-state current curve as the value of calcium conductance  $g_{Ca}$  (left) and potassium conductance  $g_K$  (right) vary.**

158 **Computational characteristics of the neuron phenotype 3.** The wild-type neuron  
 159 ( $g_{Ca} = 4.92\text{nS}$ ) displays a N-shaped steady-state current with two stable zeros corresponding  
 160 to the two values of the resting potential ( $V_*^{rest1}$  and  $V_*^{rest2}$ ) (Figure 4.A). The neuron then  
 161 has a bistable behavior (Figure 4.B). The existence of the second resting value  $V_*^{rest2}$  has  
 162 an important computational implication: the response of the cell depends on its recent  
 163 history of activity by storing information about its last input. Figure 4.C illustrates such a  
 164 phenomenon. The membrane potential of the neuron under 2000ms of a current injection  
 165 step at 5pA stabilizes at about  $-29\text{mV}$ . However, if a sufficiently high transient prestimulus  
 166 is applied, the membrane potential relaxes to its highest resting potential value  $V_*^{rest2}$   
 167 (approximately  $-8\text{mV}$ ), and finally stabilizes at about  $-6\text{mV}$  in response to the same  
 168 current injection protocol as before (current injection step at 5pA under 2000ms). The  
 169 response of the neuron to a given stimulus then depends on its history of activity. From a  
 170 dynamical system viewpoint, this is explained by the fact that the shock pulse resets the  
 171 initial condition of the system at  $V_*^{rest2}$  (Izhikevich, 2007). This can be seen in Figure 4.D:  
 172 if a transient stimulus higher than  $I_{T2}$  is applied (for example,  $I = 20\text{pA}$ ), then the new  
 173 initial condition of the voltage is at  $V_*^{rest2}$  after cessation of the current. Therefore, for  
 174 new hyperpolarization or depolarization inputs higher than  $I > I_{T1}$  (for example,  $I = 5\text{pA}$ ),  
 175 the dynamics of the voltage will converge to the stable equilibrium  $V_{2*}^{I_5}$ , and not  $V_{1*}^{I_5}$ , since  
 176  $V_*^{rest2}$  belongs to the attraction domain of  $V_{2*}^{I_5}$ . To return to  $V_*^{rest1}$ , an injection current  
 177 lower than  $I_{T1}$  has to be applied.

178 **Computational characteristics of the neuron phenotype 2.** For a reduced calcium  
 179 conductance value (for example,  $g_{Ca} = 4.12\text{nS}$ ), the neuron still exhibits a N-shaped steady-  
 180 state current, but with only one zero (Figure 5.A). The neuron then displays a bistable



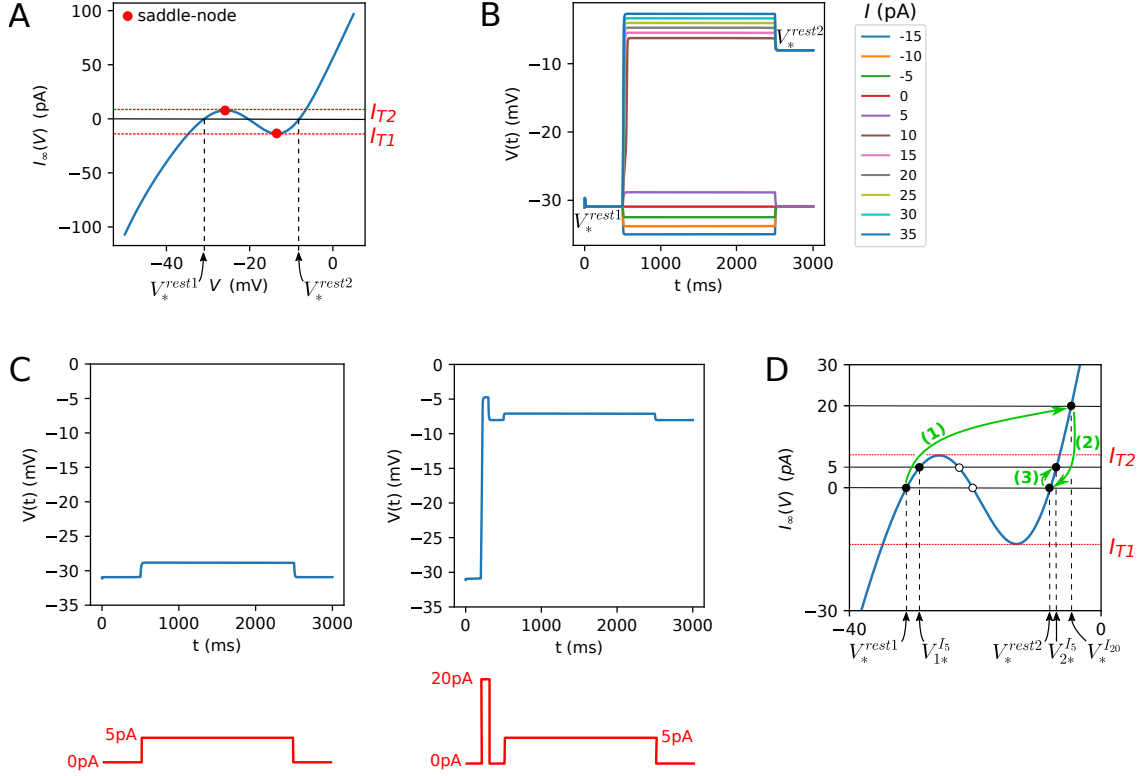


Figure 4: **Features of the wild-type bistable dynamics (phenotype 3).** (A) Wild-type steady-state current displaying a N-shape with two stable zeros corresponding to the two values of the resting potential ( $V_*^{rest1}$  and  $V_*^{rest2}$ ). The saddle points (red dots) correspond to the thresholds of the jump between the two plateau potentials of the bistable neuron, namely for  $I_{T1} \approx -13.744\text{pA}$  and  $I_{T2} \approx 7.865\text{pA}$ . (B) Bistable dynamics of the cell voltages for a series of current injections starting from  $-15\text{pA}$  and increasing to  $35\text{pA}$  by  $5\text{pA}$  increments. The jump to the upper voltage plateau occurs at  $I_{T2}$ . (C) Comparison of the voltage dynamics resulting from two different stimulation protocols. (Left) A depolarizing current step ( $5\text{pA}$ ) of  $2000\text{ms}$  duration into the neuron is applied. On cessation of the current step, the voltage stabilizes to  $V_*^{rest1}$ . (Right) A current pulse ( $20\text{pA} > I_{T2}$ ) of  $100\text{ms}$  duration is first injected into the neuron, followed by a step current ( $5\text{pA}$ ) of  $2000\text{ms}$  duration. Upon cessation of the current step, the voltage relaxes to its higher resting potential value  $V_*^{rest2}$ . (D) Diagram explaining (C). (1) A brief transient stimulus ( $20\text{pA}$ ) is applied and the voltage converges to  $V_*^{I_{20}}$ . (2) The stimulus ceases so that the voltage relaxes to  $V_*^{rest2}$  which is the new voltage initial condition. (3) A new depolarizing current step ( $5\text{pA}$ ) is applied and the voltage goes to  $V_{2*}^{I_5}$  and not  $V_{1*}^{I_5}$  since  $V_*^{rest2}$  now belongs to the basin of attraction of  $V_{2*}^{I_5}$ .

181 behavior with only one resting potential ( $V_*^{rest1}$ ) (Figure 5.B). The neuron has lost its  
182 short-term memory capacity, so the cell's response no longer reflects the history of its inputs  
183 and of its activity (Figure 5.C). The transition from two resting values to a single one is  
184 also observed experimentally in the *C. elegans* RMD neuron in mutants for voltage-gated  
185 calcium channels (Mellem et al., 2008). Moreover, compared with the wild-type phenotype,  
186 we observe that the peak amplitude of the voltages is reduced when  $g_{Ca}$  is decreasing  
187 (compare Figure 4.B with Figure 5.B), which is still in agreement with experimental data  
188 from the *C. elegans* RMD neuron (Mellem et al., 2008). Also, the value of the jump  
189 thresholds increases as  $g_{Ca}$  decreases (Figure S2), implying a loss of the overall voltage  
190 amplitude of the neuron. Indeed, as an example, the peak amplitude in the reduced and  
191 the wild-type neuron for  $I = 10\text{pA}$  is about  $-29\text{mV}$  and  $-7\text{mV}$ , respectively.

192 **Computational characteristics of the neuron phenotype 1.** When the value of  
193 the calcium conductance decreases sufficiently (for example,  $g_{Ca} = 2.42\text{nS}$ ), the steady-  
194 state current becomes monotonic (Figure 6.A), which implies the loss of the bistability  
195 of the neuron in favor of a near-linear behavior (Figure 6.B). However, it is important  
196 to note that the transition from bistable to near-linear voltage behavior is graded, in the  
197 sense that the amplitude of the voltage jump decreases in a smooth manner during the  
198 transition (Figure S3). The transition from a bistable behavior to a near-linear one is  
199 also observed experimentally in the *C. elegans* bistable RMD neuron when extracellular  
200 fluid is  $Ca^{2+}$ -free (representing approximately the case  $g_{Ca} = 0\text{nS}$ ) (Mellem et al., 2008).  
201 The same transition occurs experimentally in the bistable rabbit retinal horizontal cell of  
202 phenotype 1: calcium channels blockade results in a near-linear behavior (Aoyama et al.,  
203 2000). Finally, the current is less and less sustained as  $g_{Ca}$  decreases, making the neuron  
204 less and less sensitive to depolarizing inputs (see also Figure S3). This implies that the  
205 amplitude of the voltage is decreased when  $g_{Ca}$  is reduced.

206 Following the series of results determined and discussed above, combined with exper-  
207 imental observations from the biological literature, Figure 7 summarizes the evolution of  
208 the phenotypic dynamics of non-spiking neurons under the effect of calcium or potassium  
209 conductance variations. Experimental observations suggest, however, that these variations  
210 may compensate for each other over a certain range of functioning. The objective of the  
211 following paragraph is therefore to study these plausible compensations.

212 **Restricted range of ion channel compensations.** It is well-known that a given identi-  
213 fied neuron can maintain a specific electrophysiological feature from different combinations  
214 of its components (*e.g.* ion channels). Indeed, many experimental observations reveal that

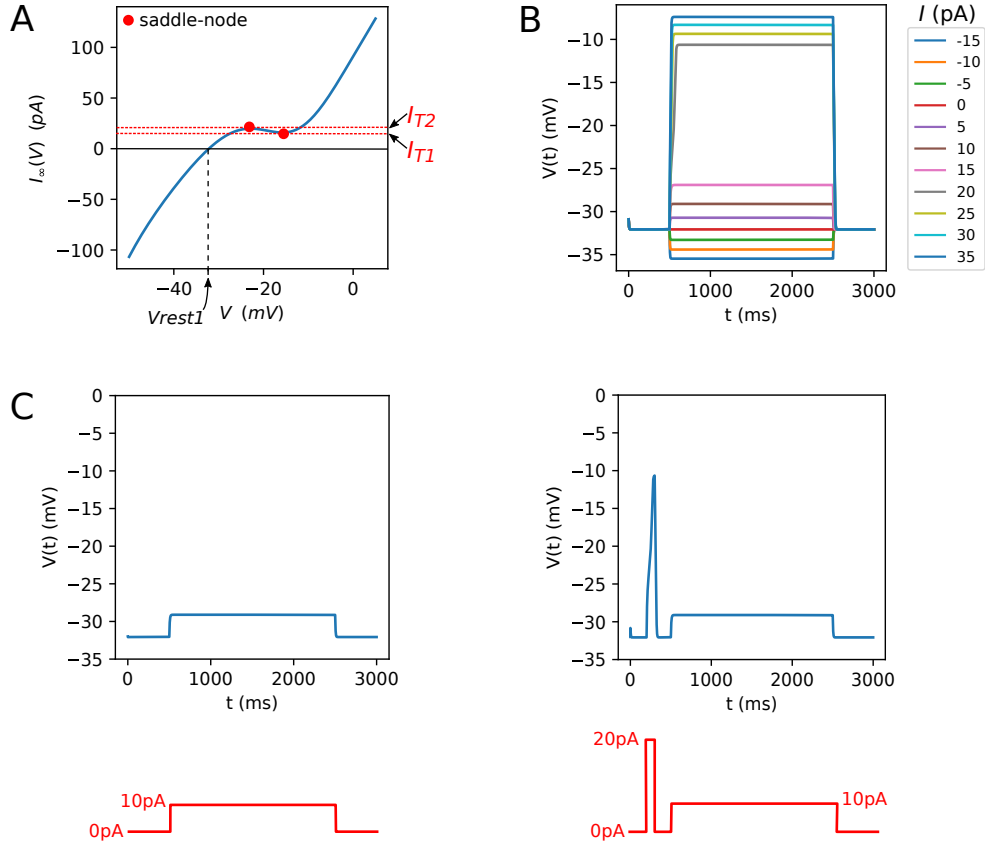


Figure 5: **Features of the bistable dynamics when calcium conductance  $g_{Ca}$  is diminished (phenotype 2).** (A) Steady-state current displaying a N-shape with only one zero corresponding to the resting membrane potential of the neuron. The saddle points (red dots) correspond to the thresholds of the jump between the two plateau potentials of the bistable neuron, namely for  $I_{T1} \approx 12.275\text{pA}$  and  $I_{T2} \approx 18\text{pA}$ . (B) Bistable dynamics of the neuron voltages for a series of current injections starting from  $-15\text{pA}$  and increasing to  $35\text{pA}$  by  $5\text{pA}$  increments. The jump to the upper plateau of voltages occurs at  $I_{T2}$ . (C) Comparison of the voltage dynamics resulting from two different stimulation protocols described in Figure 4.C. Whatever the stimulation protocol used, the neuron relaxes to a steady-state value of about  $-29\text{mV}$ : the neuron’s response does not reflect the history of its inputs.

215 a same identified neuron exhibits two to six-fold variability in its ion channels while dis-  
 216 playing similar voltage behaviors (Kamaledin, 2021; Goillard and Marder, 2021). Here  
 217 we explore and study these possible compensatory mechanisms between  $I_{Ca}$  and  $I_K$  in the  
 218 non-spiking CBM under study, from a qualitative and quantitative viewpoint.

219 It can be observed in Figure 8.A that each neuron phenotype of the model exists

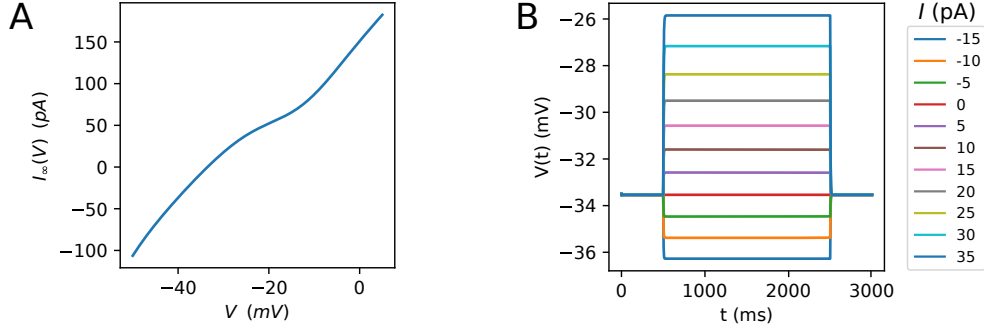


Figure 6: **Features of the neuron dynamics when calcium conductance  $g_{Ca}$  is highly reduced (phenotype 1).** (A) Steady-state current of the neuron, that exhibits a monotonic shape unlike the wild-type neuron that has a N-shape. (B) Resulting near-linear behavior of the neuron.

220 within a certain range of  $g_{Ca}$  and  $g_K$  values. As explained above, the transition between  
 221 phenotype 2 and phenotype 1 is graded in the sense that the amplitude of the voltage jump  
 222 decreases in a smooth manner during the transition from bistable to near-linear behavior.  
 223 Conversely, the transition between phenotype 2\* and phenotype 3, and between phenotype  
 224 3 and phenotype 2, occurs abruptly and immediately. The vertical dashed line indicates  
 225 the value of  $g_{Ca}$  ( $\approx 3.40$ nS) at which  $g_K$  can no longer compensate for the decrease in  $g_{Ca}$   
 226 to preserve the wild-type phenotype. Indeed, for  $g_{Ca} \approx 3.40$ nS,  $g_K$  is equal to 0 and therefore  
 227 can no longer decrease to compensate for the decrease in  $g_{Ca}$ . The neuron then switches  
 228 to phenotype 2. On the contrary, for every decreased  $g_K$  value, there are compensating  
 229 decreasing  $g_{Ca}$  values for which the wild-type phenotype is maintained. We can therefore  
 230 suggest that  $g_{Ca}$  variations (*i.e.* possible loss-of-functions of calcium channels) are more  
 231 difficult for the system to compensate than  $g_K$  variations (*i.e.* possible loss-of-functions of  
 232 potassium channels). However, in vivo, this interpretation would depend of physiologically  
 233 plausible values of  $g_K$  and  $g_{Ca}$ .

234 Furthermore, we determine a quantitative relationship between  $g_{Ca}$  and  $g_K$  (see Mate-  
 235 rials and Methods) that yield similar behaviors of the model voltages (Figure 8.B). More  
 236 specifically, we find an affine relationship between  $g_{Ca}$  and  $g_K$  given by

$$g_K = 1.6517g_{Ca} - 6.114. \quad (1)$$

237 Some examples of the different solutions obtained from this relation are shown in Figure  
 238 8.C. However, it can be noted that the more  $g_{Ca}$  decreases, the more  $g_K$  must decrease  
 239 to compensate, and the less accurately it compensates (Figure S4). Such a characteristic  
 240 can also be seen in Figure 8.C ( $g_{Ca} = 3.72$ nS,  $g_K = 0.02$ nS) on which it appears that the

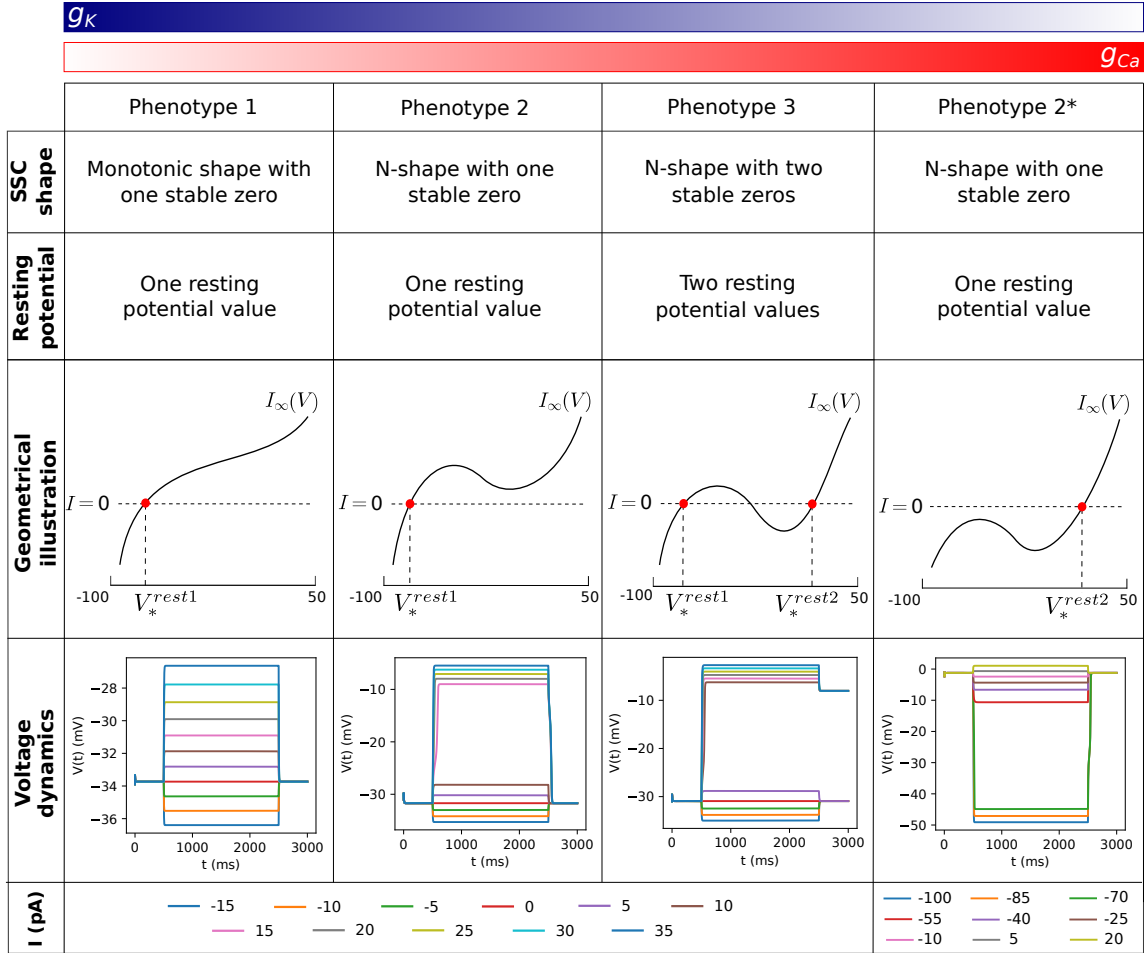


Figure 7: **General pattern of the effect of changes in calcium and potassium conductances on the non-spiking neuron dynamics.** There are three physiological behaviors of non-spiking neurons (phenotype 1, 2 and 3), while phenotype 2\* has never been observed experimentally. Variations in calcium and potassium conductances drive opposite transitions between these neuron phenotypes, involving a modification of the computational characteristics of the neuron. As an illustration, we took a well-posed retinal cone model, with a wild-type phenotype 3. Such a neuron displays two resting potential values corresponding to the intersections between the curve  $I_\infty$  and the horizontal line  $I = 0$ . The neuron is endowed with a short-term memory capacity, that is, the response of the cell depends on its recent history of activity by storing information about its last inputs. The decrease of  $g_{Ca}$  implies a unique intersection between  $I_\infty$  and the horizontal line  $I = 0$ : the bistable neuron then has only one resting potential (phenotype 2), which implies the loss of its short-term memory capacity. Finally, the decrease of  $g_{Ca}$  leads to the loss of the bistability of the neuron: it becomes near-linear (phenotype 1).

241 voltage jump occurs for relatively higher values of injection currents.

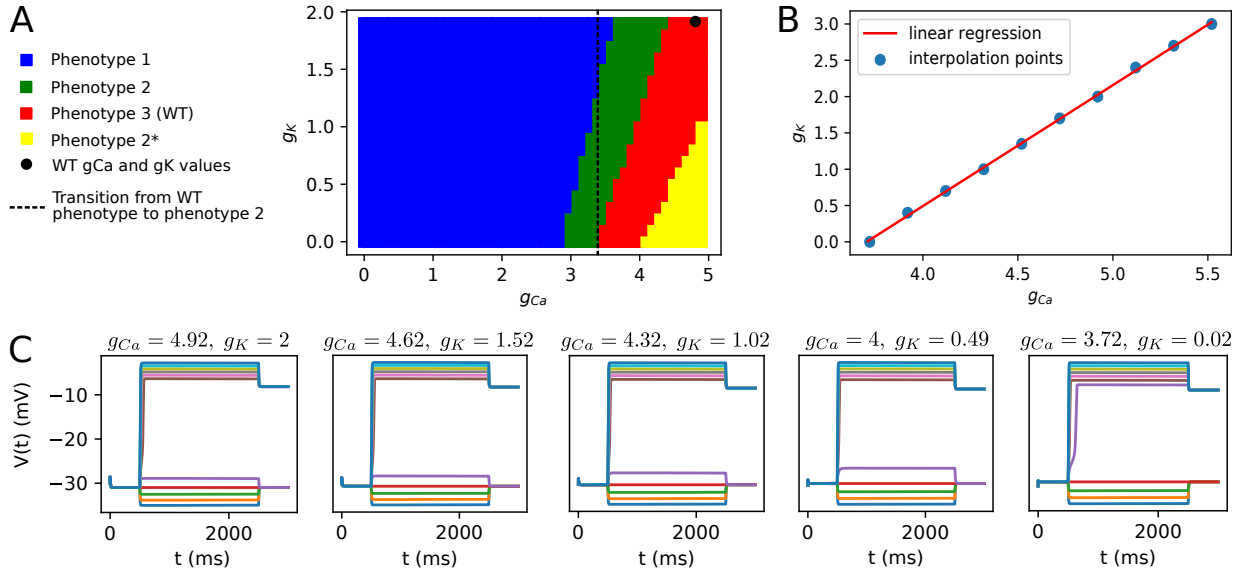


Figure 8: (A) Parameter landscape of neuron phenotypes as a function of  $g_{Ca}$  and  $g_K$ . (B) Quantitative affine relationship between  $g_{Ca}$  and  $g_K$  that gives similar voltage behaviors. (C) Example of similar voltage behaviors obtained from the relationship determined in (B), for a series of current injections starting from  $-15\text{pA}$  and increasing to  $35\text{pA}$  by  $5\text{pA}$  increments.

### 242 3 Discussion

243 Non-spiking neurons are ubiquitous in many neuronal processes and are found in a wide  
 244 variety of nervous tissues, whose the *C. elegans* and retinal networks are important exam-  
 245 ples. Based on the literature in experimental biology and on mathematical analyses we  
 246 performed, three distinct phenotypes of non-spiking neurons were determined depending  
 247 on the shape of their steady-state current. A phenotype 3 neuron is bistable with two  
 248 resting potentials (N-shaped steady-state current with two stable zeros), a phenotype 2  
 249 neuron is also bistable but with only one resting potential (N-shaped steady-state current  
 250 with one zero), while a phenotype 1 neuron is near-linear (monotonic steady-state current).  
 251 A fourth phenotype was highlighted from the mathematical analysis of a well-posed retinal  
 252 cone model. Such a phenotype is characterized by a N-shaped steady-state current with one  
 253 zero and a negative local maxima, resulting in a hyperpolarizing voltage jump. However,  
 254 to our knowledge, this non-spiking phenotype has never been observed experimentally.

255 Then, we showed that changes in calcium and potassium conductances ( $g_{Ca}$  and  $g_K$ )

drove opposite transitions between neuron phenotypes. A general pattern of the evolution of non-spiking neuron dynamics as  $g_{Ca}$  and  $g_K$  evolves was then determined, and the computational implications on the neuron dynamics were discussed. In particular, we showed that a neuron with a phenotype 3 could switch to a phenotype 2 and then 1 as  $g_{Ca}$  decreases or  $g_K$  increases. In other words, the neuron first lost its short-term memory capacity (transition from phenotype 3 to 2), then lost its bistable behavior to a near-linear one (transition from phenotype 2 to 1).

Finally, we studied the homeostatic compensatory mechanisms between  $I_{Ca}$  and  $I_K$  in the retinal cone model. In particular, we showed that there is a restricted range of ion conductance values  $g_{Ca}$  and  $g_K$  for which the phenotype and the behavior of the model are maintained. Further, we highlighted that variations in  $g_{Ca}$  are more difficult for the system to compensate than variations in  $g_K$ .

**Phenotypic classification and intra-phenotype diversity.** In this paper, we propose a classification of non-spiking neurons based on qualitative arguments derived from mathematical considerations. Specifically, as the steady-state current determines the qualitative characteristics of non-spiking neurons, the classification is based on its shape. Based on a state-of-the-art research in biology, Table 1 inventories for each phenotype class a series of experimentally identified neurons from different nervous tissues. However, it is worth noting that there are quantitative differences in behavior between neurons in each class, so that an intra-phenotype diversity exists. Indeed, as a representative example, we can compare the RIM and AIY neurons from *C. elegans* that are both of phenotype 1 (Figure S5). While AIY is more sensitive to hyperpolarizing than depolarizing inputs with a transition point around  $-30\text{mV}$ , RIM is depolarized or hyperpolarized in a smooth manner due to the lack of large sustained currents. The steady-state current of these neurons characterizes and reveals its differences (Naudin et al., 2022b), so that the addition of subclasses to differentiate qualitative features between neurons of the same class could still be done based on the steady-state current shape.

### **Implications of phenotypic changes on retinal visual information processing.**

The retina is a sensory organ located on the inner surface of the eye whose role is mainly to receive light stimuli and perform a primary visual information processing, the phototransduction. The light is captured and converted in electrical signals by the photoreceptor cells (cones and rods), then conveyed through several relays (horizontal, bipolar and amacrine cells) before reaching the ganglion cells, the last relay of phototransduction. All the retinal neurons are non-spiking except the ganglion cells, which trigger spikes. Visual information,

	Phenotype 1	Phenotype 2	Phenotype 3
Retina	Rod (Mao et al., 2003; Kamiyama et al., 2009) Amacrine (Boos et al., 1993)	Bipolar (Usui et al., 1996; Mao et al., 2003; Schilardi and Kleinlogel, 2021)	Cone (Kourennyi et al., 2004; Ko et al., 2007) Horizontal (Aoyama et al., 2000)
<i>C. elegans</i>	RIM (Liu et al., 2018) AVA (Mellem et al., 2008) VA5 (Liu and Kourennyi, 2004) PLM (O’Hagan et al., 2005) AVE (Lindsay et al., 2011) AIY (Liu et al., 2018) VB6 (Liu et al., 2017) DVC (Jiang et al., 2022) RIS (Jiang et al., 2022) Many non identified neurons (Goodman et al., 1998)	ASER (Goodman et al., 1998) AWC (Ramot et al., 2008) ASH (Geffeney et al., 2011) AFD (Liu et al., 2018) AIA (Dobosiewicz et al., 2019) Many non identified neurons (Goodman et al., 1998)	RMD (Mellem et al., 2008) Many non identified neurons (Goodman et al., 1998)
<i>Ascaris</i>	Motorneurons (Davis and Stretton, 1989a)		

Table 1: Classification of non-spiking neurons following three phenotypes. Phenotype 1 comprises near-linear neuron. Phenotype 2 bistable neurons with only one resting potential. Phenotype 3 bistable neurons with two resting potentials.

290 encoded by the spikes of ganglion cells, is then transmitted over long distances via the optic  
291 nerve formed by the axons of these cells to higher visual brain centers.

292 The electrical signal that propagates through each population of retinal cells is under-  
293 pinned by the existence of various calcium and potassium channels revealed by electro-  
294 physiological studies (Van Hook et al., 2019). Mutations in genes encoding for these ion



295 channels have been shown to be ubiquitous in retinal cells in various disorders ([Heyes et al.,](#)  
296 [2015](#); [Waldner et al., 2018](#); [Kilicarslan et al., 2021](#); [Mayama, 2014](#)). The results obtained  
297 in this paper suggest that such modifications in retinal cell ion channels could affect the  
298 integrity of the transmitted signal through phenotypic changes. How such changes in the  
299 retinal non-spiking neurons ultimately affect the ganglion cell output is then a question of  
300 interest, and will require further modeling studies that we are currently conducting.

## 4 Materials and methods

**Conductance-based models (CBMs).** In CBMs, the dynamics of the membrane potential  $V$  is described by a general equation of the form

$$C \frac{dV}{dt} = - \sum_{ion} I_{ion} + I \quad (2)$$

where  $C$  is the membrane capacitance,  $\sum_{ion} I_{ion}$  is the total current flowing across the cell membrane, and  $I$  is an applied current. The currents  $I_{ion}$  take the form

$$I_{ion} = g_{ion} m_{ion}^a h_{ion}^b (V - E_{ion})$$

where  $m$  (*resp.*  $h$ ) denotes the probability for an activation (*resp.* inactivation) gate to be in the open state;  $a$  and  $b$  are the number of activation and inactivation gates, respectively;  $g_{ion}$  is the maximal conductance associated with  $ion$  (namely the conductance of the  $ion$  channel when all the gates are open); and  $E_{ion}$  is the reversal potential, that is, the potential at which the ion current reverses its direction.

**Conductance-based model of the retinal cone cell.** The conductance-based model of the canonical retinal cone cell is based on the model developed in [Kourennyi et al. \(2004\)](#). It has four ion currents: a calcium current ( $I_{Ca}$ ), a hyperpolarization activated current ( $I_h$ ), a delayed rectifying potassium current ( $I_K$ ), and a leak current ( $I_L$ ). The parameters are expressed in the following units: mV (voltage), pA (current), nS (conductance), and ms (time). The membrane capacitance ( $C$ ) is set to 16nF. Leak current is classically described as  $I_L = g_L(V - E_L)$  and the remaining currents are described in [Table 2](#).

**Bifurcation dynamics of non-spiking CBMs.** In non-spiking CBMs, the steady-state current curve  $I_\infty$  determines the number of equilibria of the system and their values, as well as the bifurcations of the resting state along with the values to which they occur. It takes the general form

$$I_\infty(V) = \sum_{ion} I_{ion\infty}(V) \quad \text{where} \quad I_{ion\infty}(V) = g_{ion} m_{ion\infty}^a(V) h_{ion\infty}^b(V) (V - E_{ion}) \quad (3)$$

with

Ion current ( $I_{ion}$ )	$\alpha_{ion}(V)$ and $\beta_{ion}(V)$ rates	$g_{ion}$ and $E_{ion}$
$I_{Ca} = g_{Ca}m_{Ca}h_{Ca}(V - E_{Ca})$	$\alpha_{Ca}(V) = 3.1 e^{(V+16.6)/11.4}$	$g_{Ca} = 4.92$
$\frac{dm_{Ca}}{dt} = \alpha_{Ca}(1 - m_{Ca}) - \beta_{Ca}m_{Ca}$	$\beta_{Ca}(V) = 3.1 e^{(-V-16.6)/11.4}$	$E_{Ca} = 40$
$I_h = g_h(1 - (1 + 3m_h)(1 - m_h)^3)(V - E_h)$	$\alpha_{m_h}(V) = \frac{18}{(1 + e^{(V+88)/12})}$	$g_h = 3.5$
$\frac{dm_h}{dt} = \alpha_{m_h}(1 - m_h) - \beta_{m_h}m_h$	$\beta_{m_h}(V) = \frac{18}{(1 + e^{-(V+18)/19})}$	$E_h = -32.5$
$I_{Kv} = g_{Kv}m_{Kv}^3h_{Kv}(V - E_K)$	$\alpha_{m_{Kv}}(V) = \frac{5(V - 100)}{(1 - e^{-(V-100)/42})}$	$g_{Kv} = 2$
$\frac{dm_{Kv}}{dt} = \alpha_{m_{Kv}}(1 - m_{Kv}) - \beta_{m_{Kv}}m_{Kv}$	$\beta_{m_{Kv}}(V) = 9e^{(20-V)/40}$	$E_{Kv} = -80$
$\frac{dh_{Kv}}{dt} = \alpha_{h_{Kv}}(1 - h_{Kv}) - \beta_{h_{Kv}}h_{Kv}$	$\alpha_{h_{Kv}}(V) = 0.15 e^{-V/22}$	
	$\beta_{h_{Kv}}(V) = \frac{0.4125}{(1 + e^{(10-V)/7})}$	

Table 2: Summary of ion currents composing the canonical cone model.

$$x_\infty(V) = \frac{1}{1 + \exp\left(\frac{V_{1/2}^x - V}{k_x}\right)}, \quad x \in \{m, h\}.$$

321 where  $V_{1/2}^x$  and  $k_x$  are constant parameters.

322 Any stationary point of gating variables  $x \in \{m, h\}$  must satisfy  $x_* = x_\infty(V_*)$ . Replacing  
323 this into the first equation on  $V$ , fixed points  $V_*$  of such models satisfy the equation

$$I_\infty(V_*) = I. \quad (4)$$

324 In other words, equilibria  $V_*$  correspond to the intersections between the steady-state curve  
325  $I_\infty$  and a horizontal line  $I = c$  where  $c$  is a constant. There are two standard steady-state  
326 curves  $I_\infty$ , monotonic and cubic (Figure 9), each involving fundamentally different neuro-  
327 computational properties for non-spiking neurons:

328 • As shown in Figure 9.A, CBMs with a monotonic steady-state current only have  
329 one equilibrium for any value of  $I$ . Non-spiking neurons with such a steady-state  
330 current display a near-linear behavior characterized by smooth depolarizations or  
331 hyperpolarizations from the resting potential, such as the RIM and AIY neurons  
332 (Figure 1.B, left).

333 • As shown in Figure 9.B, a N-shaped curve leads to a saddle-node bifurcation. When

334  $I = c_1$ , there are 3 equilibria, noted  $V_{1*}^{c_1}$ ,  $V_{2*}^{c_1}$  and  $V_{3*}^{c_1}$ . Increasing  $I$  results in coa-  
 335 luescence of two equilibria (the stable  $V_{1*}^{c_1}$  with the unstable  $V_{2*}^{c_1}$ ). The value  $I = c_2$ ,  
 336 at which the equilibria coalesce, is called the *bifurcation value*. For this value of  $I$ ,  
 337 there exist 2 equilibria. For  $I > c_2$ , the system has only one equilibrium (*e.g.*  $I = c_3$ ).  
 338 In summary, when the parameter  $I$  increases, a stable and an unstable equilibrium  
 339 approach, coalesce, and then annihilate each other. Non-spiking neurons with a N-  
 340 shaped steady-state current display a bistable behavior characterized by a voltage  
 341 jump between the resting potential and a depolarized potential of higher voltage,  
 342 such as the AFD neuron (Figure 1.B, right).

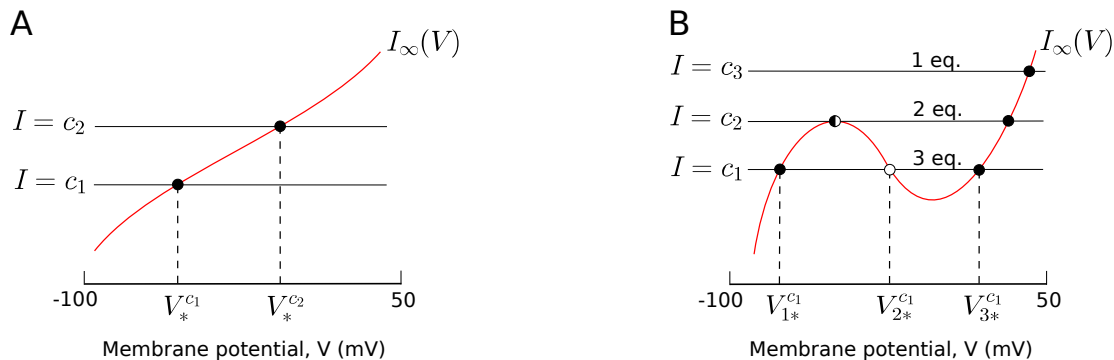


Figure 9: **Two typical shapes of the steady-state current  $V \rightarrow I_\infty(V)$ , in red.** Intersections of  $I_\infty$  and horizontal line  $I = c$  (with  $c$  constant) correspond to equilibria of the system. We denote stable equilibria as filled circles ●, unstable equilibria as open circles ○ and saddle-node equilibria as ◐. **(A)** Monotonic steady-state current.  $V_{*}^{c_1}$  and  $V_{*}^{c_2}$  correspond to equilibria for a current injection  $I = c_1$  and  $I = c_2$  respectively. **(B)** N-shaped steady-state current. The number of equilibria of the system depends on the value of  $I$ . For the sake of readability, we highlight equilibria only for  $I = c_1$ , noted  $V_{1*}^{c_1}$ ,  $V_{2*}^{c_1}$  and  $V_{3*}^{c_1}$ .

343 Therefore, it can be stated that the steady-state current determines the bifurcation  
 344 structure of non-spiking neurons and the equilibrium values of their graded responses to  
 345 particular stimuli.

346 **Procedure to build a quantitative relationship between  $g_{Ca}$  and  $g_K$ .** As explained  
 347 above, the steady-state current determines the neuro-computational features of non-spiking  
 348 neurons. Therefore, the adjustments of  $g_{Ca}$  and  $g_K$  to maintain the same neuron behavior  
 349 are carried out to preserve the wild-type steady-state current. The wild-type conductance  
 350 value of  $g_{Ca}$  is 4.92nS. For a series of decreased and increased values of  $g_{Ca}$ , we straight-  
 351 forwardly find a corresponding value of  $g_K$  for which we are as close as possible to the

352 wild-type steady-state current. Then, we perform a linear regression using Python and  
353 specific modules.

## 354 **Acknowledgements**

355 We thank Dr. Mellem and Dr. Liu for their consents to reproduce their experimental data.

## 356 **Code accessibility**

357 The code used in this paper is available at [https://gitlab.com/lois76/conductance\\_](https://gitlab.com/lois76/conductance_)  
358 [nospikingneurons\\_code](https://gitlab.com/lois76/conductance_nospikingneurons_code).

## 359 **Declaration of competing interests**

360 The authors declare no competing interests.

361 **Supplementary figures**

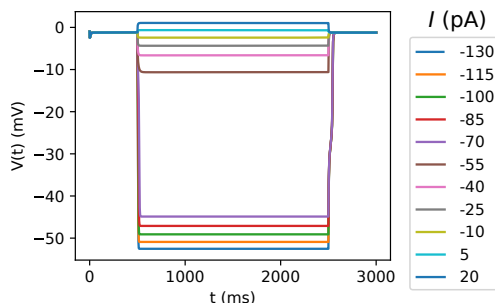


Figure S1: Example of voltage dynamics of phenotype 2\*. This phenotype is characterized by a hyperpolarizing jump of the voltage.

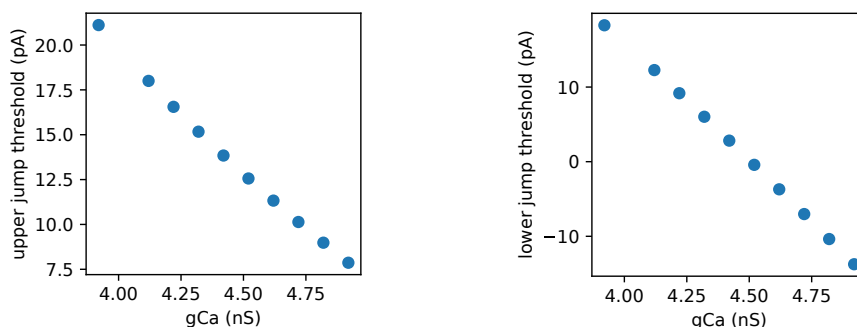


Figure S2: Calcium conductance  $g_{Ca}$  against the upper and lower jump thresholds.

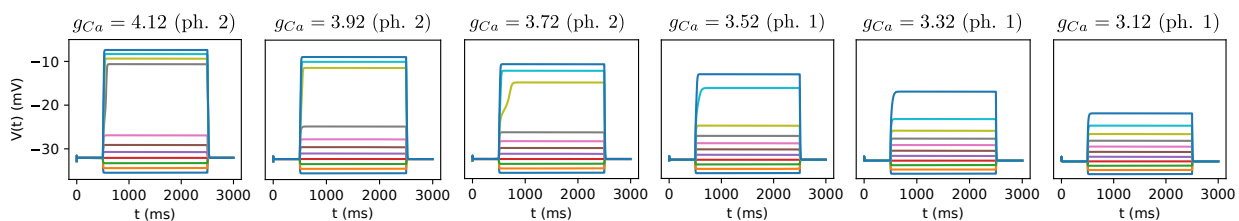


Figure S3: Evolution of the model membrane potentials for a series of current injections starting from  $-15\text{pA}$ , and increasing to  $35\text{pA}$  by  $5\text{pA}$  increments, for- different values of  $g_{Ca}$ . The transition between the phenotype (ph.) 2 and 1 is graded in the sense that the amplitude of the voltage jump decreases in a smooth manner.

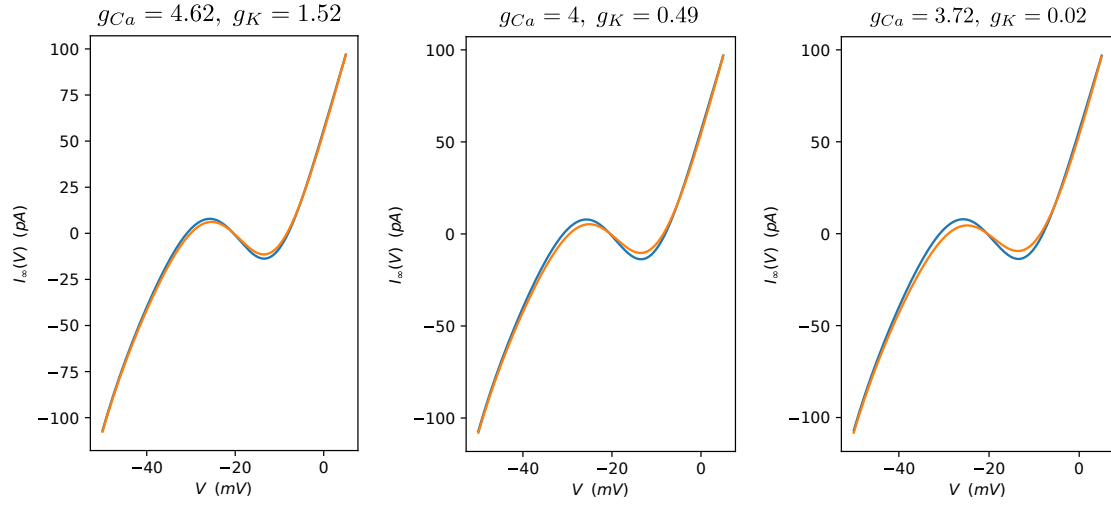


Figure S4: Wild-type steady-state current (in blue), *i.e.*  $g_{Ca} = 4.92\text{nS}$  and  $g_K = 2\text{nS}$ , against degenerate steady-state current (in orange) obtained from the equation (1) for different optimal compensatory values of  $g_{Ca}$  and  $g_K$ .

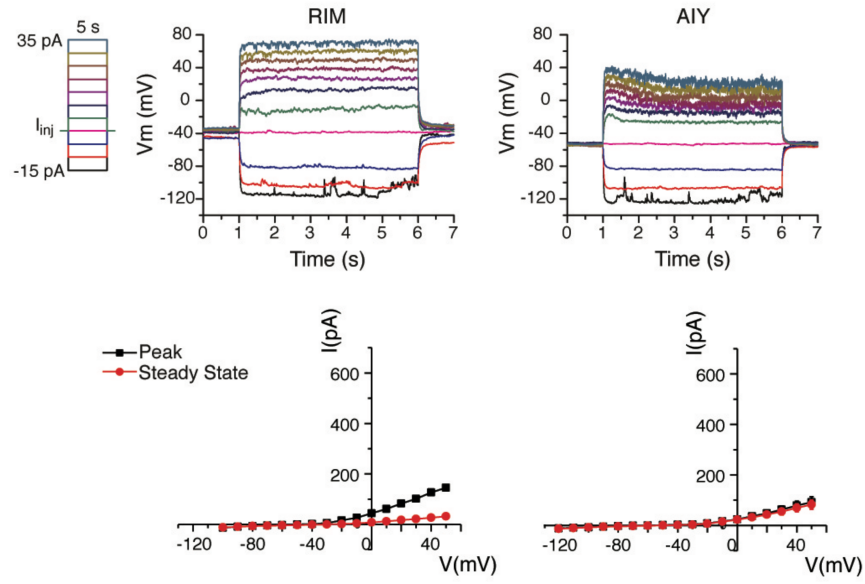


Figure S5: **(Top)** Example of the evolution of membrane potential of phenotype 1 for a series of current injections, in the space of 5 seconds, starting from  $-15$  pA and increasing to  $35$  pA by  $5$  pA increments. RIM is depolarized or hyperpolarized in a smooth manner due to the lack of large sustained currents, while AIY is more sensitive to hyperpolarization than depolarization inputs with a transition point around  $-30$  mV. **(Bottom)** I-V relationships obtained from averaged voltage-clamp recordings (RIM:  $n = 3$ ; AIY:  $n = 7$ ; AFD:  $n = 3$ ). Peak currents are measured by the absolute maximum amplitude of currents within the first 100 ms of each voltage step onset, while steady-state currents are measured by the averaged currents of the last 50 ms of each voltage step. The experimental data have been reproduced from Liu et al. (2018) with the consent of the authors.

## 362 References

- 363 P. Achard and E. De Schutter. Complex parameter landscape for a complex neuron model.  
 364 *PLoS computational biology*, 2(7):e94, 2006.
- 365 L. M. Alonso and E. Marder. Visualization of currents in neural models with similar  
 366 behavior and different conductance densities. *Elife*, 8:e42722, 2019.
- 367 T. Aoyama, Y. Kamiyama, S. Usui, R. Blanco, C. F. Vaquero, and P. de la Villa. Ionic  
 368 current model of rabbit retinal horizontal cell. *Neuroscience Research*, 37(2):141–151,  
 369 2000.
- 370 J. Art and M. Goodman. Ionic conductances and hair cell tuning in the turtle cochlea a.  
 371 *Annals of the New York Academy of Sciences*, 781(1):103–122, 1996.



- 372 A. Aussen, L. Buhry, L. Tyvaert, and R. Ranta. A detailed anatomical and mathematical  
373 model of the hippocampal formation for the generation of sharp-wave ripples and theta-  
374 nested gamma oscillations. *Journal of computational neuroscience*, 45(3):207–221, 2018.
- 375 H. Berry and S. Genet. A model of on/off transitions in neurons of the deep cerebellar  
376 nuclei: deciphering the underlying ionic mechanisms. *The Journal of Mathematical*  
377 *Neuroscience*, 11(1):1–34, 2021.
- 378 S. S. Bidaye, T. Bockemühl, and A. Büschges. Six-legged walking in insects: how cpgs,  
379 peripheral feedback, and descending signals generate coordinated and adaptive motor  
380 rhythms. *Journal of neurophysiology*, 119(2):459–475, 2018.
- 381 R. Boos, H. Schneider, and H. Wassle. Voltage- and transmitter-gated currents of all-  
382 amacrine cells in a slice preparation of the rat retina. *Journal of Neuroscience*, 13(7):  
383 2874–2888, 1993.
- 384 M. Burrows, G. Laurent, and L. Field. Proprioceptive inputs to nonspiking local interneu-  
385 rons contribute to local reflexes of a locust hindleg. *Journal of Neuroscience*, 8(8):  
386 3085–3093, 1988.
- 387 M. Czeredys. Dysregulation of neuronal calcium signaling via store-operated channels in  
388 huntington’s disease. *Frontiers in Cell and Developmental Biology*, 8:1645, 2020.
- 389 R. Davis and A. Stretton. Passive membrane properties of motoneurons and their role in  
390 long-distance signaling in the nematode *ascaris*. *Journal of Neuroscience*, 9(2):403–414,  
391 1989a.
- 392 R. E. Davis and A. Stretton. Signaling properties of *ascaris* motoneurons: graded ac-  
393 tive responses, graded synaptic transmission, and tonic transmitter release. *Journal of*  
394 *Neuroscience*, 9(2):415–425, 1989b.
- 395 M. Dobosiewicz, Q. Liu, and C. I. Bargmann. Reliability of an interneuron response  
396 depends on an integrated sensory state. *Elife*, 8:e50566, 2019.
- 397 G. Drion, T. O’Leary, and E. Marder. Ion channel degeneracy enables robust and tunable  
398 neuronal firing rates. *Proceedings of the National Academy of Sciences*, 112(38):E5361–  
399 E5370, 2015.
- 400 C. Eliasmith and O. Trujillo. The use and abuse of large-scale brain models. *Current*  
401 *opinion in neurobiology*, 25:1–6, 2014.

- 402 R. Fettiplace. Electrical tuning of hair cells in the inner ear. *Trends in Neurosciences*, 10  
403 (10):421–425, 1987.
- 404 G. D. Field and E. Chichilnisky. Information processing in the primate retina: circuitry  
405 and coding. *Annu. Rev. Neurosci.*, 30:1–30, 2007.
- 406 S. L. Geffeney, J. G. Cueva, D. A. Glauser, J. C. Doll, T. H.-C. Lee, M. Montoya, S. Kara-  
407 nia, A. M. Garakani, B. L. Pruitt, and M. B. Goodman. Deg/enac but not trp channels  
408 are the major mechano-electrical transduction channels in a *c. elegans* nociceptor. *Neu-  
409 ron*, 71(5):845–857, 2011.
- 410 F. Giovannini, B. Knauer, M. Yoshida, and L. Buhry. The can-in network: A biologi-  
411 cally inspired model for self-sustained theta oscillations and memory maintenance in the  
412 hippocampus. *Hippocampus*, 27(4):450–463, 2017.
- 413 J.-M. Goaillard and E. Marder. Ion channel degeneracy, variability, and covariation in  
414 neuron and circuit resilience. *Annual review of neuroscience*, 44, 2021.
- 415 M. B. Goodman, D. H. Hall, L. Avery, and S. R. Lockery. Active currents regulate sensi-  
416 tivity and dynamic range in *c. elegans* neurons. *Neuron*, 20(4):763–772, 1998.
- 417 S. Heyes, W. S. Pratt, E. Rees, S. Dahimene, L. Ferron, M. J. Owen, and A. C. Dolphin.  
418 Genetic disruption of voltage-gated calcium channels in psychiatric and neurological  
419 disorders. *Progress in neurobiology*, 134:36–54, 2015.
- 420 S. W. Hughes, D. W. Cope, T. I. Tóth, S. R. Williams, and V. Crunelli. All thalamo-  
421 cortical neurones possess a t-type  $ca_{2+}$  ‘window’ current that enables the expression of  
422 bistability-mediated activities. *The Journal of physiology*, 517(3):805–815, 1999.
- 423 M. J. Hurley and D. T. Dexter. Voltage-gated calcium channels and parkinson’s disease.  
424 *Pharmacology & therapeutics*, 133(3):324–333, 2012.
- 425 E. M. Izhikevich. *Dynamical systems in neuroscience*. MIT press, 2007.
- 426 J. Jiang, Y. Su, R. Zhang, H. Li, L. Tao, and Q. Liu. *C. elegans* enteric motor neurons  
427 fire synchronized action potentials underlying the defecation motor program. *Nature  
428 communications*, 13(1):1–15, 2022.
- 429 J. L. Jiménez Laredo, L. Naudin, N. Corson, and C. M. Fernandes. A methodology for  
430 determining ion channels from membrane potential neuronal recordings. In *Applications  
431 of Evolutionary Computation*, pages 15–29. Springer International Publishing, 2022.

- 432 M. A. Kamaledin. Degeneracy in the nervous system: from neuronal excitability to neural  
433 coding. *BioEssays*, page 2100148, 2021.
- 434 Y. Kamiyama, S. M. Wu, and S. Usui. Simulation analysis of bandpass filtering properties  
435 of a rod photoreceptor network. *Vision research*, 49(9):970–978, 2009.
- 436 I. Kilicarslan, L. Zanetti, E. Novelli, C. Schwarzer, E. Strettoi, and A. Koschak. Knockout  
437 of cav1. 3 l-type calcium channels in a mouse model of retinitis pigmentosa. *Scientific  
438 Reports*, 11(1):1–12, 2021.
- 439 M. L. Ko, Y. Liu, S. E. Dryer, and G. Y.-P. Ko. The expression of l-type voltage-gated  
440 calcium channels in retinal photoreceptors is under circadian control. *Journal of neuro-  
441 chemistry*, 103(2):784–792, 2007.
- 442 U. Koch, U. Bässler, and M. Brunner. Non-spiking neurons suppress fluctuations in small  
443 networks. *Biological cybernetics*, 62(1):75–81, 1989.
- 444 D. E. Kourennyi, X.-d. Liu, J. Hart, F. Mahmud, W. H. Baldrige, and S. Barnes. Recip-  
445 rocal modulation of calcium dynamics at rod and cone photoreceptor synapses by nitric  
446 oxide. *Journal of neurophysiology*, 92(1):477–483, 2004.
- 447 G. Laurent and M. Burrows. Distribution of intersegmental inputs to nonspiking local  
448 interneurons and motor neurons in the locust. *Journal of Neuroscience*, 9(9):3019–3029,  
449 1989a.
- 450 G. Laurent and M. Burrows. Intersegmental interneurons can control the gain of reflexes in  
451 adjacent segments of the locust by their action on nonspiking local interneurons. *Journal  
452 of Neuroscience*, 9(9):3030–3039, 1989b.
- 453 T. H. Lindsay, T. R. Thiele, and S. R. Lockery. Optogenetic analysis of synaptic trans-  
454 mission in the central nervous system of the nematode *Caenorhabditis elegans*. *Nature  
455 communications*, 2(1):1–9, 2011.
- 456 P. Liu, B. Chen, R. Mailler, and Z.-W. Wang. Antidromic-rectifying gap junctions am-  
457 plify chemical transmission at functionally mixed electrical-chemical synapses. *Nature  
458 communications*, 8(1):1–16, 2017.
- 459 Q. Liu, P. B. Kidd, M. Dobosiewicz, and C. I. Bargmann. *C. elegans* awa olfactory neurons  
460 fire calcium-mediated all-or-none action potentials. *Cell*, 175(1):57–70, 2018.

- 461 X.-D. Liu and D. E. Kourennyi. Effects of tetraethylammonium on kx channels and sim-  
462 ulated light response in rod photoreceptors. *Annals of biomedical engineering*, 32(10):  
463 1428–1442, 2004.
- 464 S. R. Lockery, M. B. Goodman, and S. Faumont. First report of action potentials in a c.  
465 elegans neuron is premature. *Nature neuroscience*, 12(4):365–366, 2009.
- 466 B.-Q. Mao, P. R. MacLeish, and J. D. Victor. Role of hyperpolarization-activated currents  
467 for the intrinsic dynamics of isolated retinal neurons. *Biophysical journal*, 84(4):2756–  
468 2767, 2003.
- 469 C. Mayama. Calcium channels and their blockers in intraocular pressure and glaucoma.  
470 *European Journal of Pharmacology*, 739:96–105, 2014.
- 471 J. E. Mellem, P. J. Brockie, D. M. Madsen, and A. V. Maricq. Action potentials contribute  
472 to neuronal signaling in c. elegans. *Nature neuroscience*, 11(8):865–867, 2008.
- 473 L. Naudin, N. Corson, M. Aziz-Alaoui, J. L. J. Laredo, and T. Démare. On the modeling  
474 of the three types of non-spiking neurons of the caenorhabditis elegans. *International*  
475 *Journal of Neural Systems*, page S012906572050063X, 2020.
- 476 L. Naudin, J. L. Jiménez Laredo, Q. Liu, and N. Corson. Systematic generation of bio-  
477 physically detailed models with generalization capability for non-spiking neurons. *PloS*  
478 *one*, 17(5):e0268380, 2022a.
- 479 L. Naudin, J. L. J. Laredo, and N. Corson. A simple model of non-spiking neurons. *hal*,  
480 2022b.
- 481 M. Nicoletti, A. Loppini, L. Chiodo, V. Folli, G. Ruocco, and S. Filippi. Biophysical  
482 modeling of c. elegans neurons: Single ion currents and whole-cell dynamics of awcon  
483 and rmd. *PloS one*, 14(7):e0218738, 2019.
- 484 R. O’Hagan, M. Chalfie, and M. B. Goodman. The mec-4 deg/enac channel of caenorhab-  
485 ditis elegans touch receptor neurons transduces mechanical signals. *Nature neuroscience*,  
486 8(1):43–50, 2005.
- 487 S. Onasch and J. Gjorgjieva. Circuit stability to perturbations reveals hidden variability  
488 in the balance of intrinsic and synaptic conductances. *Journal of Neuroscience*, 40(16):  
489 3186–3202, 2020.

- 490 T. O’Leary, A. C. Sutton, and E. Marder. Computational models in the age of large  
491 datasets. *Current opinion in neurobiology*, 32:87–94, 2015.
- 492 R. Publio, R. F. Oliveira, and A. C. Roque. A realistic model of rod photoreceptor for use  
493 in a retina network model. *Neurocomputing*, 69(10-12):1020–1024, 2006.
- 494 D. Ramot, B. L. MacInnis, and M. B. Goodman. Bidirectional temperature-sensing by a  
495 single thermosensory neuron in *c. elegans*. *Nature neuroscience*, 11(8):908, 2008.
- 496 A. Roberts and B. M. Bush. *Neurons without impulses: their significance for vertebrate*  
497 *and invertebrate nervous systems*, volume 6. Cambridge University Press, 1981.
- 498 R. Sarpeshkar. Analog versus digital: extrapolating from electronics to neurobiology. *Neu-*  
499 *ral computation*, 10(7):1601–1638, 1998.
- 500 G. Schilardi and S. Kleinlogel. Two functional classes of rod bipolar cells in the healthy and  
501 degenerated optogenetically treated murine retina. *Frontiers in Cellular Neuroscience*,  
502 15, 2021.
- 503 D. J. Schulz, J.-M. Goaillard, and E. Marder. Variable channel expression in identified  
504 single and electrically coupled neurons in different animals. *Nature neuroscience*, 9(3):  
505 356–362, 2006.
- 506 S. M. Silverstein, D. L. Demmin, J. B. Schallek, and S. I. Fradkin. Measures of reti-  
507 nal structure and function as biomarkers in neurology and psychiatry. *Biomarkers in*  
508 *Neuropsychiatry*, 2:100018, 2020.
- 509 W. Soofi, S. Archila, and A. A. Prinz. Co-variation of ionic conductances supports phase  
510 maintenance in stomatogastric neurons. *Journal of computational neuroscience*, 33(1):  
511 77–95, 2012.
- 512 G. E. Stutzmann. Ryr2 calcium channels in the spotlight—i’m ready for my close up, dr.  
513 alzheimer! *Cell Calcium*, 94:102342, 2021.
- 514 C. Supnet and I. Bezprozvanny. The dysregulation of intracellular calcium in alzheimer  
515 disease. *Cell calcium*, 47(2):183–189, 2010.
- 516 X. Tong, Y. Ao, G. C. Faas, S. E. Nwaobi, J. Xu, M. D. Haustein, M. A. Anderson, I. Mody,  
517 M. L. Olsen, M. V. Sofroniew, et al. Astrocyte kir4. 1 ion channel deficits contribute to  
518 neuronal dysfunction in huntington’s disease model mice. *Nature neuroscience*, 17(5):  
519 694–703, 2014.

- 520 S. Usui, A. Ishihaiza, Y. Kamiyama, and H. Ishii. Ionic current model of bipolar cells in  
521 the lower vertebrate retina. *Vision research*, 36(24):4069–4076, 1996.
- 522 M. J. Van Hook, S. Nawy, and W. B. Thoreson. Voltage-and calcium-gated ion channels of  
523 neurons in the vertebrate retina. *Progress in retinal and eye research*, 72:100760, 2019.
- 524 C. Villa, H. Suphesiz, R. Combi, and E. Akyuz. Potassium channels in the neuronal  
525 homeostasis and neurodegenerative pathways underlying alzheimer’s disease: An update.  
526 *Mechanisms of Ageing and Development*, 185:111197, 2020.
- 527 D. Waldner, N. Giraldo Sierra, S. Bonfield, L. Nguyen, I. Dimopoulos, Y. Sauvé, W. Stell,  
528 and N. Bech-Hansen. Cone dystrophy and ectopic synaptogenesis in a cacna1f loss of  
529 function model of congenital stationary night blindness (csnb2a). *Channels*, 12(1):17–33,  
530 2018.
- 531 S. R. Williams, T. I. Toth, J. P. Turner, S. W. Hughes, and V. Crunelli. The ‘win-  
532 dow’component of the low threshold ca<sup>2+</sup> current produces input signal amplification  
533 and bistability in cat and rat thalamocortical neurones. *The Journal of physiology*, 505  
534 (3):689–705, 1997.
- 535 M. Yanagi, R. Joho, S. Southcott, A. Shukla, S. Ghose, and C. Tamminga. Kv3. 1-  
536 containing k<sup>+</sup> channels are reduced in untreated schizophrenia and normalized with  
537 antipsychotic drugs. *Molecular psychiatry*, 19(5):573–579, 2014.
- 538 G. W. Zamponi, J. Striessnig, A. Koschak, and A. C. Dolphin. The physiology, pathol-  
539 ogy, and pharmacology of voltage-gated calcium channels and their future therapeutic  
540 potential. *Pharmacological reviews*, 67(4):821–870, 2015.
- 541 L. Zhang, X. Li, R. Zhou, and G. Xing. Possible role of potassium channel, big k in etiology  
542 of schizophrenia. *Medical hypotheses*, 67(1):41–43, 2006.
- 543 L. Zhang, Y. Zheng, J. Xie, and L. Shi. Potassium channels and their emerging role in  
544 parkinson’s disease. *Brain Research Bulletin*, 160:1–7, 2020.